

AC LOSSES IN SUPERCONDUCTORS*

S.L. Wipf
Atomics International
A Division of North American Rockwell Corporation
Canoga Park, California

This is a review of studies of ac losses in superconductors. In a paper¹ published three years ago we read in reference to previous work that "there is frequently considerable disagreement between results obtained with comparable samples in similar experimental conditions (ratios of 10^2 or even of 10^4)." I took this as a challenge.

Looking into this more closely revealed surprising agreement if results are expressed properly. Of course now there are many more results available.

Interest in ac losses is largely a practical one, because:

- 1) Present-day technology, with conventional conductors, uses ac. It is easiest simply to replace the conductor.
- 2) There are special applications, ideal for superconductivity and inherently ac, such as gyroscopes, linear accelerators, etc.
- 3) In a wider sense ac is encountered in any transient, such as charging and discharging of magnet coils, and it is this aspect which interests the accelerator builder most.

The type I superconductor plays an insignificant role in most of these applications. This was decided over a generation ago, because the critical fields and currents are too small (Pb with a critical field of 550 Oe at 4.2°K alone has kept a place).

Type II superconductors almost shared the same fate and it took 30 years before their usefulness was rediscovered, perhaps luckily, for otherwise all of us would probably worry about different problems and there would not have been this Summer Study.

The reason for this is that an ideal type II superconductor becomes resistive at even lower fields and currents, as we see (bottom right-hand graph in Fig. 1) in the critical current vs field diagram. Only a nonideal, or imperfect, type II superconductor carries transport current in high fields as is illustrated at the top right of Fig. 1.

In the mixed state (between H_{c1} and H_{c2} in the magnetization curve on the left side of Fig. 1) the bulk superconductor admits magnetic flux (Fig. 2). This flux is bundled into fluxoids by means of a corresponding current pattern, which is shown (top of Fig. 2) together with the internal field.⁹⁷ The field maxima are at the normal cores of the fluxoids. This current pattern represents, in a sense, the maximum current density which can be carried in every place of the material. All the currents are flowing in little circles and there is no net current flow. If a transport current is impressed it will have to flow in addition to these currents and therefore create resistance.⁹⁸ At the same time, the fluxoids having no preferred places in an ideal material start moving under the influence of Lorentz forces.

*This is an expanded version of a talk given at the Applied Superconductivity Conference in Austin, Texas, 1967 [see J. Appl. Phys. 39, 2538 (1968)].

In an imperfect superconductor the superconducting parameters (T_c , H_{c1} , etc.) have locally different values. We illustrate (bottom of Fig. 2) the local variations of the energy gap Δ . If now a transport current is impressed, the flux structure will adjust its position in a way that the current density in the transport current direction is in places where Δ is larger whereas the lower Δ regions carry current in the opposite direction. Eventually a fluxoid distribution is reached which represents the largest transport current possible. We can also see that as soon as the fluxoids start to move under the influence of Lorentz forces a large dissipation will set in because the transport current will have to flow in regions where it exceeds the critical supercurrent density and therefore creates resistance. This way of looking at what is usually called "flux pinning" is particularly suitable for our ac loss discussion. We are all used to thinking in terms of Ohm's law and the resistance mentioned above is actually measured in certain experiments which we shall discuss.

Our task then is to review ac losses in imperfect type II superconductors.

Of the vast literature covering ac studies in superconductors we have to make a choice in the light of this introduction. Our main interest is in studies which emphasize directly ac losses; it is inevitable that the phase transition under ac conditions is also of great interest in this context. Many ac losses are connected with specific applications, and finally we have to include papers dealing with other special topics which are closely related.

We list the references as follows, vaguely in order of their importance within each group:

1. Ac losses, experimental: references 1 to 32. Of these 1 to 19 provide data which can be compared to each other (see Figs. 14 and 20 and accompanying tables). Other references whose main emphasis puts them into different groups but which also belong here are 34, 36, 59, 60 and 84.
2. Ac losses, theoretical approach and calculations: references 33 to 44; also of interest here are 9, 10, 22 and 23.
3. Ac phase transition (critical ac current): references 45 to 56 and also 6, 8, 19, 27, 57, 58 and 62.
4. Ac studies in coils and incidental to coil performance: references 57 to 62 and also 4, 10, 11 and 33. Reference 63 concerns losses in an adiabatic demagnetization apparatus, and Refs. 64 and 65 deal with superconducting transformers.
5. Studies of cavities and high frequencies: references 66 to 77. Of these only 66 to 73 address themselves specifically to the problem of losses, whereas the others simply report Q's and not further explained differences in Q values. Reference 83 may also be of interest here. Since superconducting cavities have been studied quite extensively prior to the arrival of type II superconductors one should include Ref. 78, which is a review of this earlier work.
6. Special topics: references 79 to 90. This includes resonances,⁸⁰ flux jumps,⁸⁷ current distribution,^{88,89} resistance in increasing field,⁸¹⁻⁸³ and special experimental methods.⁸⁴⁻⁸⁶

Without stating any special claims we hope that this list is reasonably complete in Groups 1-3. It is naturally less so in subsequent groups and in fact quite eclectic in Group 6.

After these introductory remarks we look at the electrodynamic distinction between a normal conductor and a superconductor.

First, we recapitulate the situation in a normal metal: Everybody knows Ohm's law; ρ is the resistivity, j the current density (Table I). We have two of the Maxwell

TABLE I
Normal Conductor

Ohm's law	$E = \rho j$
Maxwell equation	$\text{Curl } B = 4\pi j$ $\text{Curl } E = -\dot{B}$
Diffusion equation	$\nabla^2 B = \frac{4\pi}{\rho} \dot{B}$

equations (units such that $c = 1$). We put Ohm's law into the lower of these equations and substitute the result into the curl of the upper equation to obtain the diffusion equation which we know from heat conduction. The electromagnetic diffusivity is the inverse of the factor $4\pi/\rho$.

For an alternating field the solution for the induction inside a conductor is given in Fig. 3, with λ being the penetration depth (Fig. 3). We find that the amplitude falls off into the interior and at the same time the phase shifts (as indicated by the imaginary component). The penetration depth is inversely proportional to $\sqrt{\omega}$, a well-known fact.

About type I superconductors we shall not say much (Table II). Ohm's law is valid for the normal electrons, the current being made up of a normal and a supercurrent, and London's equation applies for the superconducting part. There is a kind of $L di/dt$

TABLE II
Type I Superconductor

$$\left. \begin{aligned} E &= \rho j_n \\ E &= \frac{\delta}{\delta t} \Lambda j_s \end{aligned} \right\} j = j_n + j_s$$

$$\frac{j_s}{j_n} = \frac{\rho}{\Lambda 2\pi \nu}$$

$$\Lambda \approx 10^{-31}$$

$$\rho \approx 10^{-20}$$

$$j_n \text{ negligible for } \nu < 10^{10} \text{ Hz}$$

term. Only Λ is so very small that j_n is practically zero even if di/dt is not. If the process which led to the diffusion equation is followed, a similar equation is obtained and the solution shows j_s/j_n to be proportional to $\rho/(\Lambda \text{ times frequency})$. With order of magnitude values for Λ and ρ it turns out that j_n is negligible below 10^{10} Hz. At these frequencies, which reach into the far infrared region, the radiation energy becomes comparable to the energy gap. This means that in the process of the absorption the Cooper pairs are destroyed.

For lower frequencies there are no losses inside the superconductor. A type II superconductor behaves as a type I below H_{c1} , and therefore this result applies also.

In a type II superconductor Ohm's law (if we can call it that) still looks the same, with the important modification that $\rho = 0$ if $j < j_c$ (Fig. 4). This makes all the difference. If j exceeds the critical value, ρ will change very rapidly through many orders of magnitude in a very small current interval. Since j_c is large, it is a good practical assumption that j in this equation is constant and, therefore, ρ is proportional to E and with E it is proportional to dB/dt .

The Maxwell equation involving curl B is given for a plane slab with X direction into the superconductor. (We can assume a constant j_c independent of B which will turn out to be an adequate simplification.)

A field will penetrate into the material with the illustrated slope, inducing the critical current density everywhere in the penetration layer ($dB/dx = 4\pi j_c$). If the field moves in the opposite direction it will induce the critical current density in the opposite direction. The field inside changes in the manner indicated with arrows until the opposite amplitude is reached.

Note that at the same external H , between the extremes, the internal field is different depending on whether the field goes up or down. This gives the hysteresis in the magnetization curve.

The diffusion equation is obtained as before, but $\nabla^2 B$ is essentially constant for the dB/dt values under consideration because of the proportionality between ρ and dB/dt .

This proportionality between ρ and dB/dt may need some elaboration and also some experimental corroboration (Fig. 5). If we consider a cylinder in a parallel field large enough to penetrate to the center and increasing at the rate dH/dt , one has inside $dB/dt = dH/dt$ outside (to a near approximation).

We can work out the electric field at a point r by the Maxwell equation: circumference times $E =$ flux change inside. One gets $E = \frac{1}{2}r dH/dt$. We know that $j = j_c =$ constant. It follows that $\rho \propto dH/dt$. If now a longitudinal transport current is applied we must get a voltage drop following Ohm's law with an average value of $\rho \propto (b/j_c) dH/dt$. We may call this the "dynamic resistivity."

A word about the averaging factor. In our example we deduce that $\rho = 0$ at the center of the specimen ($r = 0$), and Kirchhoff's law would then require the transport current to flow through the center with infinite density. But with the total current density being limited to a value close to j_c , the transport current will flow over the whole cross section, with resistance everywhere. Without getting involved in the complicated problems of the details of this current flow^{88,89,99} we assume a uniform distribution and obtain the average value given. We can get the same results by using solutions of the diffusion equation, known from the thermal equivalent (H corresponds to T and the thermal diffusivity α to $\rho/4\pi$). The advantage is that many mathematical solutions exist; in this case we need the temperature difference between the center of a specimen (cylindrical, infinitely long) and its surface which has a uniformly increasing (or decreasing) temperature.

Let us look at the experimental results shown in Fig. 6. Rayroux, Itschner and Müller⁸¹ made measurements on a bifilar coil in an increasing external field. The transport current through the coil creates a voltage which we see here. Observe that there is no voltage until the field, which completely penetrates the wire, is reached, because then there is a completely superconducting core which does not see dH/dt and carries the transport current without loss. Afterwards we encounter the resistivity just calculated. The same is true on reducing the field from 15 kG; there is no

resistance until the penetration field (~ 14 kG) is reached.

Comparison of these results with other results is made in Table III. In the first column the radius of the cylinder is given, a 10 mil wire measured by Taquet⁶¹ (using the same geometry which was subsequently used by Rayroux⁸¹) and a 5 mil wire mentioned in Fig. 6. The second column gives the resistivity divided by dH/dt . The last column shows for comparison the ratio $\rho j_c / (b dH/dt)$. The difference in these numbers is partly a factor due to different geometry and partly uncertainty in the applicable j_c values. The first case (Lubell and Wipf⁸³) which is calculated, using the thermal equivalent, gives the same factor as presented in Fig. 5.

TABLE III
Resistivity in Type II Superconductors

	b (cm)	$\rho / (dH/dt)$ ($\Omega \cdot \text{cm} \cdot \text{sec} \cdot \text{Oe}^{-1}$)	$\rho j_c / (b dH/dt)$ ($\Omega \cdot \text{A} \cdot \text{cm}^{-2} \cdot \text{sec} \cdot \text{Oe}^{-1}$)
Lubell and Wipf (Ref. 83)	6.5×10^{-1}	10^{-13}	2.5×10^{-9}
Taquet (Ref. 61)	1.27×10^{-2}	4.5×10^{-16}	3.6×10^{-9}
Rayroux et al. (Ref. 81)	6.35×10^{-3}	2.66×10^{-16}	2.6×10^{-9}

What can we use from this for our ac discussion? Realizing that ρ in the normal state is $\approx 10^{-6} \Omega \cdot \text{cm}$ or more, we see that up to dH/dt corresponding to at least several kHz this way of looking at a superconductor will be adequate. Remembering our peculiar diffusion equation this means that the loss per cycle is independent of frequency and to a large extent independent of the wave shape, as is in fact observed.

To complete our background discussion we distinguish four different regions depending on the peak ac field. In each of these regions, I, II, III, IV, we find a different behavior. In the top half of Fig. 7 we see a magnetization curve. An ideal type II superconductor would follow the solid line to the lower critical field H_{c1} and then the dashed curve to the upper critical field H_{c2} . Between H_{c2} and H_{c3} only a superconducting surface sheath remains with a negligible contribution to the magnetization. On reducing the field this curve would be retraced. The imperfect superconductor follows the magnetization curve shown by the solid line.

For each region is indicated (in the lower half of the figure) how the field penetrates a cylindrical specimen. In region I, below H_{c1} , no flux penetrates. The shielding is done by a surface current. We do not expect any losses here because the bulk does not see any ac field. Whatever losses appear (in spite of this) should be proportional to the surface exposed to the ac field. In region II, between H_{c1} and the penetration field, a surface current still remains, but the ac field now penetrates to a certain depth below the surface. This flux is pushed in and out against the pinning forces and this gives the loss. An equivalent way of putting it: the changing field in this layer creates a resistance (which we have discussed) and this resistance in the presence of the critical current density (which does the shielding) causes the loss. We shall later calculate this loss. In the magnetization curve we describe a loop as indicated by shading, and this area constitutes the loss per cycle. The core of the superconductor does not see the changing fields and therefore we again expect the losses to be proportional to the surface exposed to the ac field.

In region III, between H_p , which depends on the thickness and the critical current density of the specimen, and the upper critical field, the whole specimen sees the field, and the losses become proportional to the volume. The losses usually become

large enough to destroy superconductivity. This has not encouraged much research in this region. (The recent interest in using superconducting magnets in accelerators where cyclic field variations of 50 kG amplitude or more are required has stimulated fresh investigations,^{94,95} but at a very low frequency of 1 Hz or less.)

At this point one should mention that there is practically no difference whether the surface field is produced externally or by an ac current flowing parallel to the axis. In the case of a current the field is directed circumferentially parallel to the surface. (The current will flow in the shielding layer.)

Experiments are often made on the effect of having a dc field superimposed on the ac. One might then go through a magnetization hysteresis loop as indicated in Fig. 7. In that case, the ac does not penetrate the whole specimen; the loss behavior is similar to region II. As a rule the losses are higher because the smaller critical currents allow more flux to enter and leave cyclically.

For completeness we mention region IV, between H_{c2} and H_{c3} , where only the surface remains superconducting. For most high field superconductors straight ac amplitudes reaching above H_{c2} are unavailable, and there is little applied interest in this region. The study of this region yields information about the surface current. We shall not further discuss this region.

Preceding a discussion of the results we review the various methods employed to study ac losses. The most popular method is the calorimetric one, shown in Fig. 8. The heat produced is measured by the amount of helium boiled off by the specimen which is immersed in it. The sensitivity is moderate, about 1 mW. This usually requires several meters of wire as a specimen. A bifilar arrangement is preferred, in order to have a uniform relation between current and surface field. Another way to overcome low sensitivity is by the use of higher frequencies. It is well established^{5,6,9} that the total loss increases linearly with frequency (up to over 20 kHz) as mentioned before. The loss per cycle is independent of frequency.

Next in popularity is an electrical method. By measuring the current and voltage across the specimen with the true phase relation between the two, one obtains the loss by the integral of the product over one cycle. It has been established,¹ by measuring the same specimens, that the two methods are equivalent.

The independence of frequency of the loss per cycle makes static methods possible. The area under a full cycle of the magnetization curve will give the loss (Fig. 9). Again there are measurements¹³ on the same material showing agreement between results obtained by this method or a dynamic one. In the chosen example²⁰ the shape of the material, V_3Ga in powder form, makes this an ideal method.

A very high sensitivity is obtained by more sophisticated calorimetric methods⁵ (Fig. 10). Here the specimen, a 3 in. to 4 in. long piece of wire, is in a vacuum chamber and both of its ends are in thermal contact with the bath. The three thermometers fixed on the wire give a temperature profile along the wire. From this information and the thermal conductivity, the heat produced in the wire is calculated. A heater fixed near the center serves for calibration, which in this case means a determination of the thermal conductivity.*

Some more exotic methods should also be mentioned. They may not give quantitative results which can easily be compared with others but they sometimes expose new aspects otherwise unobserved.

* Reference 5 includes values for the thermal conductivity in NbZr at temperatures between 2 and 4.2°K.

One such method is the study of L-C circuits made of superconductors. In Fig. 11 we see two pictures of decaying oscillations (in an L-C circuit of PbBi). One portion indicates ac losses, the other, a very much slower decay, the loss in the dielectric. These losses are due to flux pinned in the surface. There seems to be an indication here that below a certain amplitude the ac losses become zero. As we shall see later, this might be expected, but there are no other reports of similar observations.

Measurements of the Q values of rf cavities also belong here.

Figure 12 shows another static method in which mechanical forces or torques are measured. A rotating field can be represented as two crossed ac fields 90° out of phase. In this way we can use a torque meter to measure the pinning. This method is most useful in region III, for fully penetrating fields. Then the torque is directly proportional to the pinning strength, which can be highly anisotropic as is seen in Fig. 13 for a vanadium single crystal. We see a plot of the torque, which is proportional to the pinning strength, versus angle — one full rotation — and at various fields.

We now come to discussion of the over-all results. It is clear that losses measured in region I and II should be given as loss per unit surface vs the peak field which this surface sees. In Fig. 14 we show the results for Nb alloys. This includes — here undistinguishable — NbZr (20-40% Zr) and NbTi (20-50% Nb). Each of these twenty-odd curves represents a whole set of measurements, usually one curve per publication. So you are looking at the result of a considerable amount of work. The curves are labelled a, b, c, through v, w. The references and explanatory information for each curve are found in Table IV. It is remarkable that this graph covers 10 orders of magnitude in the loss values. H_{c1} of these materials is around 100 Oe. We are therefore in region I below this value.

TABLE IV
Ac Losses in Nb Alloys (see Fig. 14)

<u>Curve</u>	<u>Reference</u>	<u>Investigators</u>	<u>Materials</u>	<u>Dimensions</u>	<u>Geometry</u>	<u>Method</u>	<u>External Ac</u>
a	9	Di Salvo	Nb 25% Zr	10 mil wire, 10- 20 in.	Coil open circuit	Boil- off	Ac field
b	9	Di Salvo	Nb 25% Zr } NbTi }	5 mil wire	Coil open circuit	Boil- off	Ac field
c	9	Di Salvo	NbTi	2.5 mil wire	Coil open circuit	Boil- off	Field
d	13	Nakayama and Takano	Nb 25% Zr	5 mil (x 2 lower) 10 mil } 20 mil }	70 mm long bundle 5 mm diam	Boil- off magnet- ization hyster- esis	Field
e	10 (Fig. 5)	Pech and Fournet	Nb 25% Zr	10 mil } 20 mil }	Various coils	Boil- off	Current
f	8	Rhodes et al.	Nb 25% Zr	10 mil	Bifilar wide spacing	Boil- off	Current

TABLE IV (continued)

<u>Curve</u>	<u>Reference</u>	<u>Investigators</u>	<u>Materials</u>	<u>Dimensions</u>	<u>Geometry</u>	<u>Method</u>	<u>External Ac</u>
g	19	Taylor	Nb 25% Zr	10 mil 6 in. long	Straight	Current voltage	Current
h	11	Pech and Fournet	Nb 25% Zr	10 mil 6 m long	Bifilar	Current voltage	Current
i	6	Bogner and Heinzel	Nb 33% Zr	9 mil 3 m	Bifilar	Current voltage	Current
k	1	Pech et al.	Nb 25% Zr	10 mil	Bifilar	Boil- off phase shift	Current
l	9 (Figs. 2,4)	Di Salvo	Nb 25% Zr	10 mil	Bifilar	Current voltage	Current
m	15	Claude and Mailfert	Nb 25% Zr	10 mil	Bifilar widely spaced	Current voltage	Current
n	4 (Fig. 4) (Fig. 7)	Jones and Schenck	Nb 25% Zr	8.5 mil 125ft long 10 mil 680ft long	Coil	Boil- off	Current
o	1	See k	Different sample				
p	14	Damman et al.	NbTi	10 mil 10 m long	Bifilar spaced	Current voltage	Current
q	14	Damman et al.	Nb 25% Zr	10 mil	Bifilar		
r	12 (Sample 2,3)	Takano	Nb 25 % Zr	10 mil 20 mil 10 m long	Bifilar	Boil- off	Current
s	12 (Sample 4,5)	Takano	Nb 48% Zr	5 mil 10 mil			
t	12 (Sample 1)	Takano	Nb 25% Zr	5 mil			
u	7	Heinzel	Nb 25% Zr	0.19 mm 3.6 m long	Bifilar	Magnet- ization	
v	5	Wissemann et al.	Nb 33% Zr	10 mil		Calori- metric (thermal conduc- tivity)	Current
w	5 (Fig. 5)	Wissemann et al.	Nb 25% Zr	10 mil			

The curves v and w represent all of the measurements of Wisseman, Boatner and Low⁵ (see Fig. 10). The three single points labelled i may be somewhat suspect; all other points of that work follow curve i.

Region III is roughly above ~ 2000 Oe. The penetration field H_p depends on the radius and the critical current density. The kink in curve a indicates H_p for a 10 mil wire, in curve b for a 5 mil wire, and in curve c for a 2.5 mil wire. If we plot these three branches of region III in terms of loss per unit volume they fall close together.

Between 150 and 2000-3000 Oe we have region II which we shall discuss in more detail. We see that towards the top the curves all have roughly the same slope, close to H^3 . Towards smaller fields they bend downwards to a greater degree and meet region I which has very low losses. We shall see that this trend is reasonably well understood, when we follow the calculations (Table V).

TABLE V
Calculation of Loss per Cycle

Magnetization hysteresis loop	$\frac{1}{4\pi} \oint H dB$
Poynting vector	$\frac{1}{4\pi} \int_{\text{surface}} E \times H df$
Joule loss	$\int_{\text{volume}} E j dv$
Pinning forces	$\int F_p dx dv$

We calculate the losses by using any one of four equivalent methods:

- 1) Area under magnetization curve: Integral over one full cycle of $H dB$.
- 2) By considering the Poynting vector: We observe how much energy goes through the surface into the sample and how much comes out, by forming the integral of $E \times H$ over one cycle and the surface.
- 3) Joule heating: By integrating the product Ej over the volume.
- 4) By working out the energy lost by the movement of flux lines against the pinning forces, $F_p dx$ over one cycle and then integrating over the volume.

We find all of these calculations in the literature. Notably London³³ and Bean³⁴ have presented such calculations (see also Refs. 9, 35).

Let me very quickly review the joule heating method. Illustrated in Fig. 15 is the penetration depth which during each cycle is filled with flux first in one direction and then in the other. The current density always opposes the electric field, therefore there is always loss. The total flux which passes r during one cycle is here $B_s (1 - r/d)(D - r)$; multiply this by j_c . The integration gives the answer for loss per cycle: a factor $\times B_s^3/j_c$ and in technical units the factor becomes $4.22 \times 10^{-9} \text{ J}\cdot\text{A}/\text{Oe}^3\cdot\text{cm}^4$. If j_c is not constant with field we have further smaller terms.³⁷ B_s is the induction near the surface.

Now we establish the relation between B_s and the external field H (Fig. 16). We

know that the surface can carry a surface current density which is partly due to the ideal equilibrium magnetization and partly due to separate flux pinning qualities of the surface. This means: as we lower the field, B_s does not immediately change as it would if we only had the ideal surface step. We first have to reverse the surface pinning current and reach a lower field H' before B_s starts changing. The total surface step which is operative here is denoted by ΔH .

We therefore have the complete loss formula where B_s is replaced by $(H - \Delta H)$. This formula gives the losses in region II (loss in erg, H in Oe, j_c in A/cm²). If we insert a current density of 4×10^5 A/cm² which is an average value for most of the Nb alloys represented in Fig. 14 (j_c varies between 10^5 and 10^6 A/cm²) we have finally the very simple form given in Fig. 16 for the losses.

The values for ΔH in Fig. 17 were measured by Ullmaier and Gauster⁷⁹ who also pointed out its importance for ac losses.³⁸ Using these ΔH values in conjunction with the formula of Fig. 16 gives curves 2 and 3 of Fig. 18. The shading indicates the majority of the curves in Fig. 14. Also indicated here as curve 1 is H^3 . For comparison the loss in copper (resistivity $\sim 10^{-8}$ $\Omega \cdot \text{cm}$) which goes as H^2 is given. Of course the loss per cycle depends on the frequency, because of the penetration depth.

We see that the superconductor is better by orders of magnitude. Unfortunately the peak fields are not high enough for most of us to get excited about this.

Figure 19 shows a comparison between $(H - \Delta H)^3$ and H^n since most authors discuss their losses in terms of n . Here, then, are unadulterated values as quoted for measurements over the indicated range. The comparison is with curves 2 and 3 of Fig. 18 and also with a constant value of 100 and 200 Oe for ΔH . Ullmaier and Gauster's measurements of ΔH were for ΔH less than 500 Oe; the dashed part is an extrapolation by me. So much for region II.

Many measurements have been made on pure Nb (Table VI, Fig. 20) and some on pure Pb (Fig. 21). Nb has a lower critical field of ~ 1100 - 1420 Oe, depending on purity.¹⁰⁰ Therefore most measurements seen here are in region I going over on the right-hand side into region II very steeply.

Figure 14 showed losses per cycle up to 10^{-3} J/cm². The bulk of the curves in Fig. 20 lie below the curves in Fig. 14. The large scatter indicates that the surface treatment of the specimens is of great importance. The loss mechanism is somewhat different and there is no quantitative theory worked out yet.^{101,36} Qualitatively we can visualize the origin of these losses in the following way: Whatever flux is trapped in the superconductor will somewhere pierce the surface. Each fluxoid will somewhere enter the specimen and at some other point, leave it. At these entry and exit points the outside field is of course seen. The action of the ac field tries to shift these points around. The surface has a pinning force which then leads to losses.

The experimental evidence that this viewpoint is correct includes the fact that specimens without trapped flux have the lowest losses, as seen in Fig. 22 for Pb and Nb. We see the losses vs the field during cool-down.

As mentioned with the L-C circuit decay (Fig. 11), a cutoff amplitude is expected below which fluxoids are truly pinned without movement. Only tenuous experimental evidence exists as yet.

So far we have talked simply about losses and without exception about losses in materials and under conditions of applied interest. There are, of course, many other ac effects; let me mention just one which easily qualifies for our discussion.

In Fig. 23 is shown what can be interpreted as a cooperative phenomenon in the

TABLE VI
Losses in Pure Niobium

<u>Curve</u>	<u>Reference</u>	<u>Investigators</u>	<u>Specific Dimensions</u>	<u>Geometry</u>	<u>Method</u>	<u>External Ac</u>
a	17	Easson and Hlawiczka	Hollow cylinder slit (o.d. 3/4 in.)	Mech. polished	Boil-off	Field
b	8 (Sample 1)	Rhodes et al.	10 mil 3½ m	Bifilar	Boil-off	Current
c	17	Easson and Hlawiczka	Same as (a) as machined			
d	8 (Sample 2)	Rhodes et al.	Same as (b)		Different sample	
e	8 (Sample 3)	Rhodes et al.	Same as (b), (d)		Specimen annealed	
f	6 (Figs. 7,8)	Bogner and Heinzl	0.15 mm 5.1 m	Bifilar	Voltage	Current
g	14	Dammann et al.	0.25 mm 10 m	Bifilar	Current voltage	Current
h	2 (Fig. 2)	Buchhold and Molenda	5 mm x 25 mm	Cylinder	Calorimetric (spec. heat)	Field (parallel)
i	3	Buchhold and Molenda	Same as (h)			
k	12	Takano	10 mil 10 m long	Bifilar	Boil-off	Current
l	12	Takano	6 mil	Bifilar		
m	3	Buchhold and Molenda	Same as (i)		Best specimen	
n	2 (Fig. 3)	Buchhold and Molenda	Same as (h)	Different specimen from same ingot		
o	16 (Fig. 5a)	Rocher	4 mm diam 55 mm long Sample 1 $\Gamma = 1030$	Cylinder	Calorimetric (see Ref.2)	Field
p	16 (Fig. 4d)	Rocher	#4 $\Gamma = 120$	Cooled in earth field		
q	16 (Fig. 4b)	Rocher	#2 $\Gamma = 850$	Cooled in earth field		
r	16 (Fig. 4d)	Rocher	Same as (p)	Cooled in zero field		
s	16 (Fig. 4b)	Rocher	Same as (q)	Cooled in zero field		

fluxoid structure. In region III of a weak pinner we see loss maxima which look like resonances of the whole flux lattice. This observation is very sensitive also to anisotropy of pinning.

For accelerator applications the interest is clearly in region III and to simplify or complicate matters - according to whether you look at it as an experimentalist or as a theorist - the emphasis lies on the performance of a complete coil.

A good starting point for calculations in these cases is the paper by Hancox,³⁹ even if the match with experimental results (as we shall hear in subsequent papers^{94,95}) is apparently not yet ideal. I feel inclined to think that the dynamic resistance, which will be discussed in more detail by Rayroux, may contribute much to the understanding of region III.

The real limiting factor evidenced in region III is the phase transition or the ac critical current (since we talk almost always about self-fields of ac currents) which is intimately connected with the large losses.

Figure 24 gives the available experimental material and some expected limits. The plot gives frequency vs peak ac critical field. The points represent experiments (see Table VII). The curves, numbered 1-5, are theoretical limits discussed below.

TABLE VII
Critical Ac Currents

<u>Curve or Point</u>	<u>Reference</u>	<u>Investigators</u>	<u>Material</u>	<u>Dimension and Geometry</u>
a	48 (Fig. 4c)	Finzi and Grasmehr	Nb 25% Zr	10 mil, 6.8 cm, straight (in perpendicular dc field of 7650 Oe)
b	48 (Fig. 4a)	Finzi and Grasmehr		(In perpendicular dc field of 3100 Oe)
X	6 (Fig. 3)	Bogner and Heinzl	Nb 33% Zr	0.23 mm, 3 m, bifilar
Δ	47 (Figs.1,2)	Young and Schenk	Nb 25% Zr	5 mil, 3/8 in., straight
O	47 (Figs.1,2)	Young and Schenk	Nb 25% Zr	10 mil, 3/8 in., straight
□	47 (Figs.1,2)	Young and Schenk	Nb 25% Zr	20 mil, 3/8 in., straight
	45	Rogers	Nb 25% Zr different suppliers	8 cm, straight (50 Hz only) diameters (from low to high field) in mm: 0.191; 0.254; 0.269; 0.403; 0.254; 0.888.
+	19 (Fig. 3)	Taylor	Nb 25% Zr	10 mil, 6 in., straight

We can think of three types of limitations of the critical current:

- 1) There is a superconducting limit, equal to the short sample dc critical current given by maximum flux pinning. The arrows indicate these values (calculated for the samples used) for a 5 mil wire (Δ), a 10 mil wire (O),

and a 20 mil wire (\square) of NbZr. It is not surprising that this seems to be an upper limit.

- 2) Runaway heating. With increasing losses the temperature of the specimen rises, this leads to higher losses, to a further temperature rise, etc. If this process is not self-limiting, by reaching an equilibrium with the cooling capacity, the runaway heating will destroy superconductivity (Ref. 48, curves a and b, attempts an explanation of this kind).

As a criterion for runaway heating one might choose the start of film boiling, if, as usual, the specimen surface is in contact with liquid helium. Taking as a rough figure 1 W/cm^2 as the transition from nucleate to film boiling we obtain curve (1) as the locus for average ac losses of this magnitude. The return from film to nucleate boiling takes place at a much lower value of $\sim 0.1 \text{ W/cm}^2$ represented by curve (2). Keeping in mind that during the whole ac cycle dissipation only takes place during about half the time but then at twice the value, we reach 1 W/cm^2 already for curve (3). Curves 1-3 are all calculated with $j_c = 4 \times 10^5 \text{ A/cm}^2$ and $\Delta H = 0$. If values for ΔH are taken from Fig. 17, then curve (2) is modified into curve (4).

Although these curves and the experimental points have the same slope, the discrepancy otherwise is large enough to leave some doubt whether this is the whole story. The heat transfer from a surface into liquid helium¹⁰² happens to be far too complicated to be representable in one or two figures. It may be that a direct visual observation through high speed photography will eventually provide a satisfactory answer.

- 3) Instability. Coils often have a lower critical current caused by instabilities (coil degradation). A similar phenomenon is expected in straight wires of sufficient thickness, provided the self-field at the surface reaches a value high enough for instabilities to occur ($> \sim 4 \text{ kG}$). If the frequency is above $\sim 20 \text{ Hz}$ we may assume adiabatic conditions for the flux penetration process and calculate a flux jump field as curve (5) according to Ref. 103 (assuming $H < H_p$). This same phenomenon should also limit the dc critical current but below 10 Hz the process is no longer adiabatic and the limit, therefore, more difficult to calculate. So far this limit has not been experimentally observed because the currents were not high enough, i.e., the sample not thick enough.*

It is perhaps best to conclude with these experimental suggestions lest somebody thinks that all problems are solved.

In summary we can say that we understand reasonably well the losses in region II.

We have only two material properties j_c and ΔH influencing the losses. (Any other variables such as temperature, applied dc field, etc., influence the losses through these material properties.) On the other hand, we have the amount of surface and the peak field as external variables and they are influenced by the particular geometry.

In conclusion we can safely say that this study shows that there is very little immediate need for more loss measurements in pure Nb or Nb alloys (unless, of course, with specific applications in mind). However, there are very few measurements on the brittle materials Nb₃Sn, V₃Ga, etc. But we ought to increase our understanding of ΔH . This may open the door towards reducing ac losses.

* For instabilities observed under ac conditions, in a cylindrical tube, see Ref. 87.

REFERENCES

Group 1

1. T. Pech, J.P. Duflot, and G. Fournet, Phys. Letters 16, 201 (1965).
2. T.A. Buchhold and P.J. Molenda, Cryogenics 2, 344 (1962).
3. T.A. Buchhold and P.J. Molenda, General Electric Progress Report No. 1; AF-33(657)-11722; BPSN 63-6899-737102 (1963), pp. 47-52.
4. C.H. Jones and H.L. Schenk, in Advances in Cryogenic Engineering (Plenum Press, 1962), Vol. 8, p. 579.
5. W.R. Wisseman, L.A. Boatner, and F.J. Low, J. Appl. Phys. 35, 2649 (1964).
6. G. Bogner and W. Heinzl, Solid-State Electronics 7, 93 (1964).
7. W. Heinzl, Phys. Letters 20, 260 (1966).
8. R.G. Rhodes, E.C. Rogers, and R.J.A. Seebold, Cryogenics 4, 206 (1964).
9. F. DiSalvo, Avco Everett Research Laboratory Report AMP-206 (1966).
10. T. Pech and G. Fournet, Cryogenics 7, 26 (1967).
11. T. Pech and G. Fournet, in Advances in Cryogenic Engineering (Plenum Press, 1968) Vol. 13, p. 60.
12. N. Takano, in Proc. First Intern. Cryogenic Engineering Conference, Kyoto, 1967, (Heywood-Temple, 1968), p. 184.
13. Y. Nakayama and N. Takano, *ibid.*, p. 186.
14. C. Dammann, E. Santamaria, J. Maldy, and L. Donadieu, Phys. Letters 24A, 574 (1967).
15. M.L. Claude and M.A. Mailfert, Phys. Letters 24A, 150 (1967).
16. Y.A. Rocher and J. Septfonds, Cryogenics 7, 96 (1967).
17. R.M. Easson and P. Hlawiczka, Phys. Stat. Sol. 23, K129 (1967).
18. R.M. Easson and P. Hlawiczka, Brit. J. Appl. Phys. 18, 1237 (1967).
19. H.F. Taylor, Appl. Phys. Letters 11, 169 (1967).
20. H.R. Hart and P.S. Swartz, General Electric Progress Report, loc. cit. Ref. 3, pp. 19-25.
21. H.R. Hart and P.S. Swartz, Bull. Am. Phys. Soc. 9, 252 (1964).
22. H.A. Ullmaier, Phys. Stat. Sol. 17, 631 (1966); see also Phys. Letters 21, 507 (1966).
23. T.W. Grasmehr and L.A. Finzi, IEEE Trans. MAG2, 334 (1966).
24. J. Huret, Rev. de Phys. Appl. 2, 133 (1967).
25. J.L. Zar, Rev. Sci. Instr. 34, 801 (1963).
26. J.L. Zar, J. Appl. Phys. 35, 1610 (1964).
27. R.A. Kamper, Phys. Letters 2, 290 (1962).
28. R.A. Kamper and P.F. Chester, in Proc. 8th Intern. Conf. Low Temperature Physics, London, 1962 (Butterworth, 1963), p. 371.
29. R.M. Easson and P. Hlawiczka, Phys. Letters 20, 333 (1966).
30. R.J. Slaughter, E.C. Rogers, and R. Grigsby, Phys. Letters 23, 214 (1966).
31. A.N. Lord, J. of Metals 16, 90 (1964).
32. B.F. Figgins and T.A. Shepherd, Nature 202, 890 (1964).

Group 2

33. H. London, Phys. Letters 6, 162 (1963).
34. C.P. Bean, Phys. Rev. 36, 31 (1964).
35. H.R. Hart and P.S. Swartz, General Electric Progress Report, loc. cit. Ref. 3, pp. 5-18.
36. T.A. Buchhold, Cryogenics 3, 141 (1963).
37. H. Voigt, Phys. Letters 20, 262 (1966).
38. H.A. Ullmaier, Phys. Letters 21, 507 (1966).
39. R. Hancox, Proc. IEE (London) 113, 1221 (1966).
40. I.M. Green and P. Hlawiczka, Proc. IEE (London) 114, 1329 (1967).
41. H.J. Fink, Phys. Rev. 161, 417 (1967).
42. A. Mailfert, Phys. Letters 25A, 247 (1967).
43. F. Irie and K. Yamafuji, Phys. Letters 24A, 30 (1967).
44. P. Graneau, Phys. Letters 5, 15 (1963).

Group 3

45. E.C. Rogers, Phys. Letters 5, 317 (1963).
46. E.C. Rogers, Phys. Letters 22, 365 (1966).
47. F.J. Young and H.L. Schenk, J. Appl. Phys. 35, 980 (1964).
48. L.A. Finzi and T.W. Grasmehr, IEEE Trans. MAG 3, 277 (1967).
49. A. Mailfert, G. Fournet, and J. Huret, Phys. Letters 7, 227 (1963).
50. V.V. Sychev, V.B. Zenkevich, V.V. Andrianov, and V.A. Al'tov, Soviet Phys. Doklady 9, 978 (1965).
51. R.M. Easson, P. Hlawiczka, and J.M. Ross, Phys. Letters 20, 465 (1966).
52. R.M. Easson and P. Hlawiczka, Phys. Letters 25A, 53 (1967).
53. R.M.F. Linford, Phys. Letters 17, 18 (1965).
54. M.A.R. LeBlanc and H.G. Mattes, Solid State Commun. 4, 267 (1966).
55. J. Maldy, E. Santamaria, and L. Donadieu, Phys. Letters 25A, 318 (1967).
56. J.E. Mercereau and L.T. Crane, Phys. Rev. Letters 9, 381 (1962).

Group 4

57. R.C. Wolgast, H.P. Hernandez, P.R. Aron, H.C. Hitchcock, and K.A. Solomon, in Advances in Cryogenic Engineering (Plenum Press, 1968), Vol. 8, p. 601.
58. C. Grenier and B. Elschner, Philips Res. Reports 20, 235 (1965).
59. J. Rufenacht and A. Steinemann, Z. Angew. Math. Phys. 16, 713 (1965).
60. S. Kurtin, S. Foner, and E.J. McNiff, Jr., Rev. Sci. Instr. 38, 600 (1967).
61. B. Taquet, J. Appl. Phys. 36, 3250 (1965).
62. R.W. Meyerhoff, J. Appl. Phys. 38, 3913 (1967).
63. A.C. Anderson, W.R. Roach, and R.E. Sarwinski, Rev. Sci. Instr. 37, 1024 (1966).

64. A. Mailfert and G. Fournet, *Compt. Rend.* 258, 2271 (1964).
65. T. Pech, *Rev. Gen. Elec.* 76, 271 (1967).

Group 5

66. L. Rinderer, J. Ruefenacht, and A. Susini, *Phys. Letters* 2, 119 (1962).
67. J. Ruefenacht and L. Rinderer, in Proc. 8th Intern. Conf. Low Temperature Physics, London, 1962 (Butterworth, 1963), p. 326.
68. W.M. Fairbank, J.M. Pierce, and P.B. Wilson, *ibid.*, p. 324.
69. J.M. Pierce, H.A. Schwettman, W.M. Fairbank, and P.B. Wilson, in Proc. 9th Intern. Conf. Low Temperature Physics, Columbus, Ohio, 1964 (Plenum Press, 1965), Part A, p. 396.
70. C.R. Haden and W.H. Hartwig, *Phys. Letters* 17, 106 (1965).
71. J.M. Victor, G.A. Persyn, and W.L. Rollwitz, *Cryogenics* 7, 119 (1967).
72. C.R. Haden, *Proc. IEEE* 54, 417 (1966).
73. C.R. Haden, W.H. Hartwig, and J.M. Victor, *IEEE Trans. MAG* 2, 331 (1966).
74. J.M. Victor, G.A. Persyn, and W.L. Rollwitz, *Cryogenics* 7, 119 (1967).
75. N.I. Krivko, *Soviet Phys.* 9, 1033 (1965).
76. Nguyen Tuong Viet, *Compt. Rend.* B264, 1227 (1967); *ibid* B258, 4218 (1964).
77. F. Biquard, A. Septier, and P. Grivet, *Electronics Letters* 3, 47 (1967).
78. E. Maxwell, in Progress in Cryogenics (Heywood & Co., 1964), Vol. 4, p. 123.

Group 6

79. H.A. Ullmaier and W.F. Gauster, *J. Appl. Phys.* 37, 4519 (1966).
80. J.C. Renard and Y.A. Rocher, *Phys. Letters* 24A, 27 (1967).
81. J.M. Rayroux, D. Itschner, and P. Müller, *Phys. Letters* 24A, 351 (1967).
82. W.F. Druyvesteyn, *Phys. Letters* 25A, 31 (1967).
83. M.S. Lubell and S.L. Wipf, *J. Appl. Phys.* 37, 1012 (1966).
84. M. Garbuny, M. Gottlieb, and J. Conroy, *J. Appl. Phys.* 36, 1177 (1965).
85. M. Gottlieb and M. Garbuny, *Rev. Sci. Instr.* 35, 641 (1964).
86. S.L. Wipf, Conference Type II Superconductors, Cleveland, Ohio, 1964; Westinghouse Scientific Paper 64-1J0-280-Pl.
87. D.A. Gandolfo and C.M. Harper, *J. Appl. Phys.* 37, 4582 (1966).
88. M.A.R. LeBlanc, *J. Appl. Phys.* 37, 3 (1966).
89. P. Martinoli, J.L. Olsen, and P. Zoller, *Phys. Letters* 20, 12 (1966).
90. G.M. Foster, *Phys. Rev. Letters* 11, 122 (1963).

Recent ac references*

91. H.F. Taylor, Phys. Rev. 165, 517 (1968); see also Ref. 19.
92. S.V. Odenov and V.A. Shukman, Soviet Physics JETP Letters 7, 125 (1968).
93. D.A. McLachlan, Physik Kondensierten Materie 7, 226 (1968).
94. W.B. Sampson, R.B. Britton, G.H. Morgan, and P.F. Dahl, in Proc. 6th Intern. Conf. High Energy Accelerators, Cambridge, Mass., 1967 (CSFTI, Springfield, Va., 1967), p. 393.
95. W.S. Gilbert, R.E. Hintz, and F. Voelker, Lawrence Radiation Laboratory Report UCRL-18176 (1968).

Other references

96. J.W. Heaton and A.C. Rose-Innes, Cryogenics 4, 85 (1964).
97. U. Essmann and H. Träuble, Phys. Letters 24A, 526 (1967).
98. W. Klose, Phys. Letters 8, 12 (1964).
99. C.J. Bergeron, Jr., Appl. Phys. Letters 3, 63 (1963).
100. D.K. Finnemore, T.F. Stromberg, and C.A. Swenson, Phys. Rev. 149, 231 (1966).
101. J.I. Gittleman and B. Rosenblum, J. Appl. Phys. 39, 2617 (1968).
102. R.D. Cummings and J.L. Smith, in Pure and Applied Cryogenics (Pergamon Press, 1966), Vol. 6, p. 85.
103. S.L. Wipf and M.S. Lubell, Phys. Letters 16, 103 (1965).

*The list (Refs. 1-90) was completed Dec. 1967.

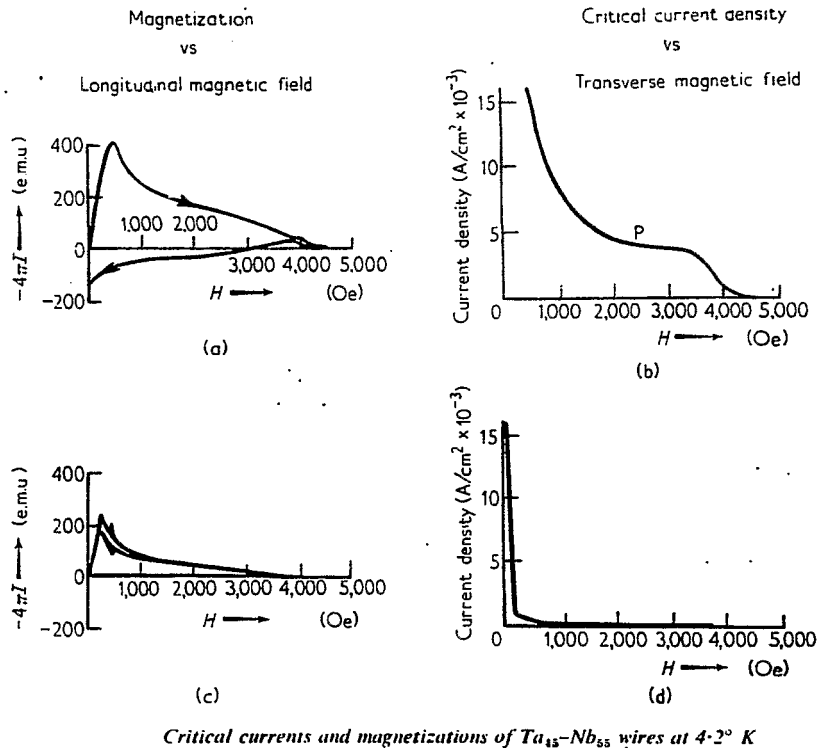


Fig. 1. Phenomenological difference between a type II superconductor with pinning (top) and without pinning (bottom) (Ref. 96).

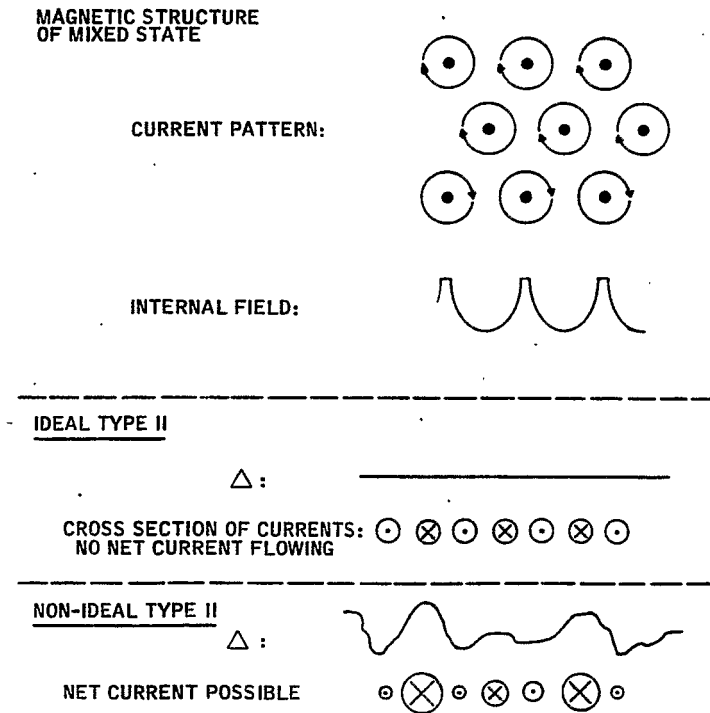


Fig. 2. Microscopic difference between ideal (no pinning) and imperfect (pinning) type II superconductor.

FOR A SURFACE FIELD $H_0 e^{i\omega t}$

THE SOLUTION OF THE DIFFUSION EQUATION GIVES

$$B = H_0 e^{\lambda x} e^{i\omega t}$$

WITH $\lambda = -[2\pi\omega/\rho]^{1/2} (1+i)$

PENETRATION DEPTH $[2\pi\omega/\rho]^{-1/2}$

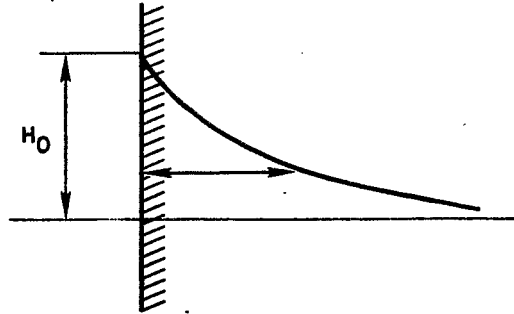


Fig. 3. Illustrating the penetration of an ac field into a normal conductor.

$$E = \rho j \quad \rho = 0 \text{ FOR } j \leq j_c$$

PRACTICALLY: $j = \text{CONST.} = j_c$; $\rho \propto dB/dt$

$$dB/dx = 4\pi j_c$$

$$\nabla^2 B = \frac{4\pi}{\rho} \dot{B} (\cong \text{CONST})$$

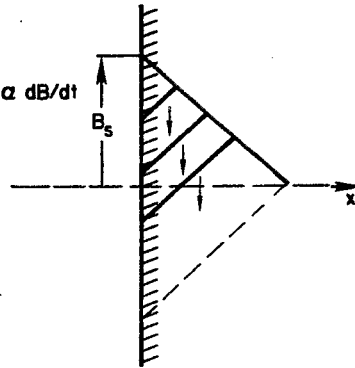
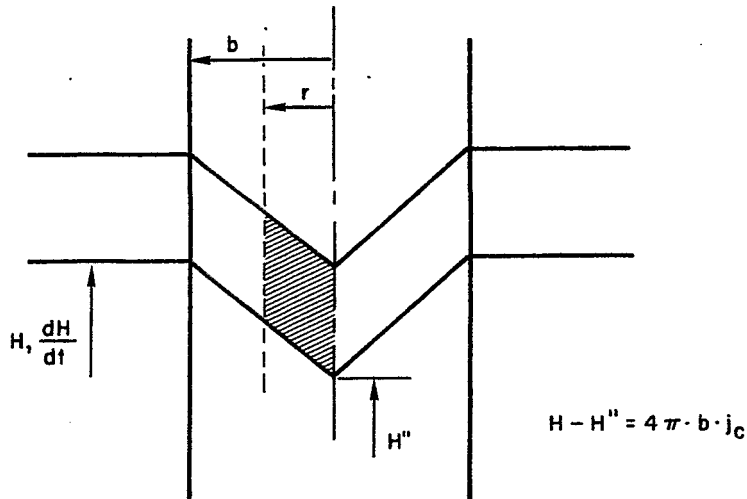


Fig. 4. Illustrating the penetration of an ac field into a type II superconductor with pinning.



$$H - H'' = 4\pi \cdot b \cdot j_c$$

TEMPERATURE EQUIVALENT

$$H \sim T$$

$$\frac{\rho}{4\pi} \sim \alpha = \frac{k}{c}$$

$$\alpha \nabla^2 T = \dot{T}$$

$$T - T'' = \frac{b^2}{4\alpha} \cdot \frac{dT}{dt}$$

$$2\pi r E = \pi r^2 \frac{dB}{dt}$$

$$E = \frac{r}{2} \frac{dH}{dt} = \rho j_c$$

$$\rho_{av} = \frac{b}{4j_c} \frac{dH}{dt}$$

Fig. 5. Dynamic resistivity of a cylindrical superconductor (type II, strong pinning) in parallel, steadily increasing field.

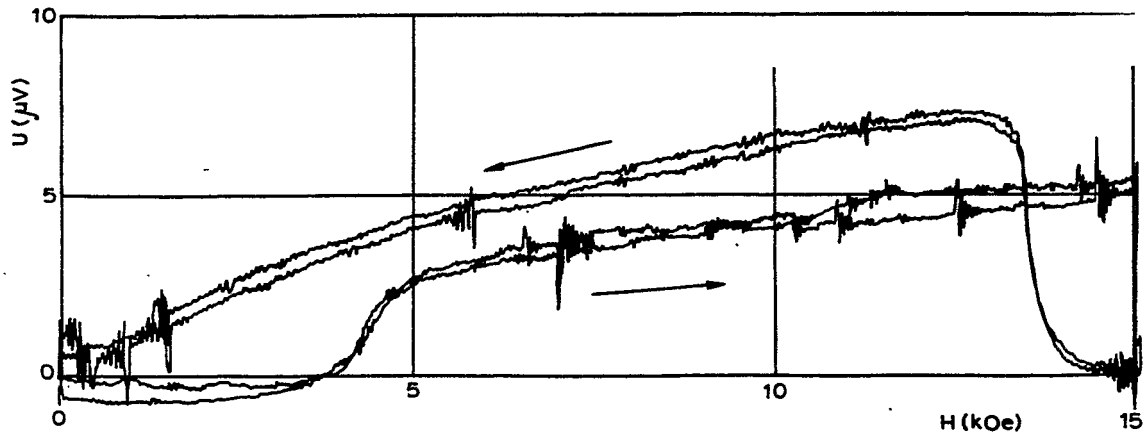


Fig. 6. Measurement of the dynamic resistance of a bifilar coil in coaxial, changing field (Ref. 81).

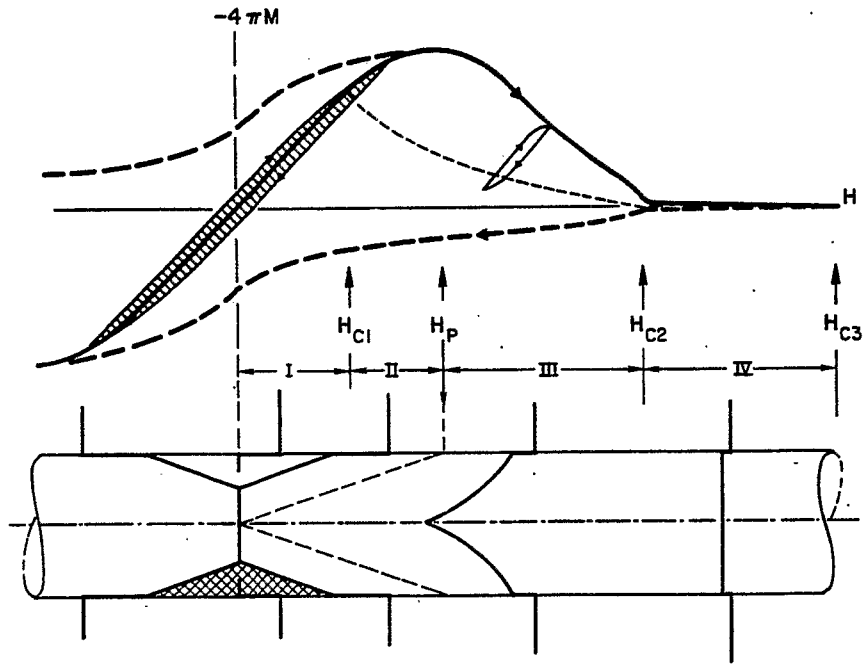


Fig. 7. Four ac loss regions.

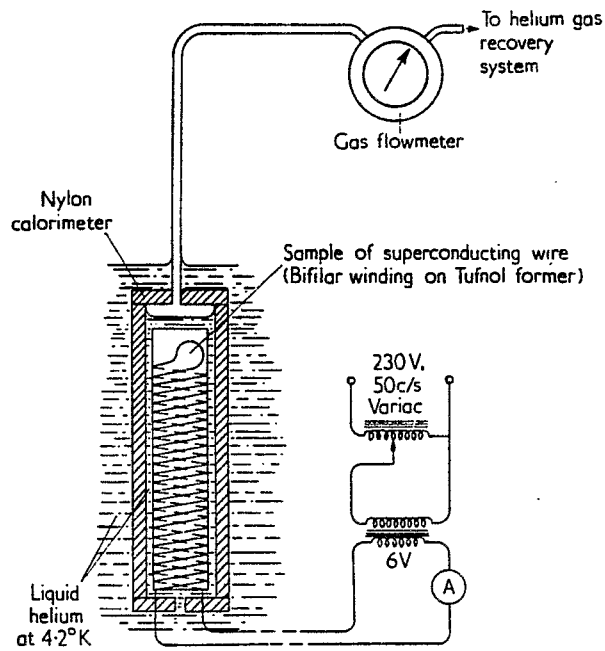


Fig. 8. Experimental method: boil-off calorimeter (Ref. 8).

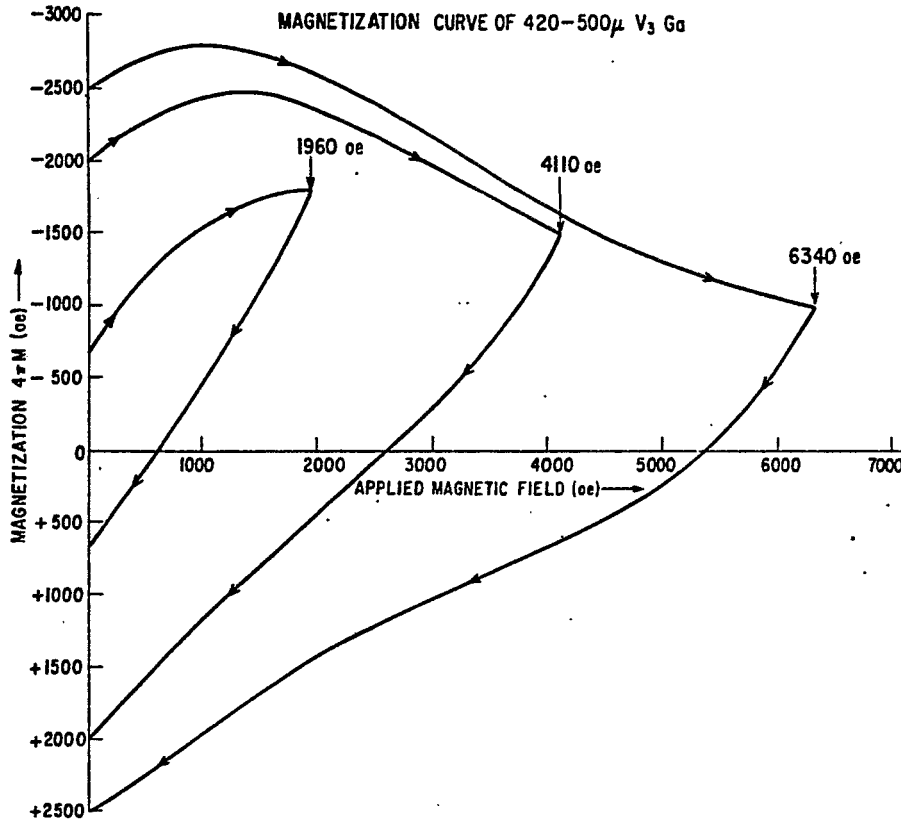


Fig. 9. Experimental method: hysteresis of magnetization loop (Ref. 20).

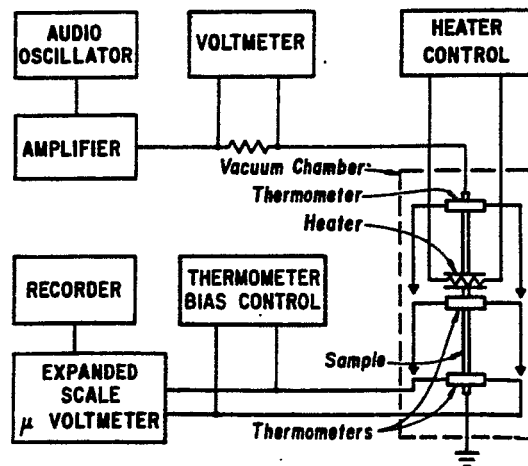
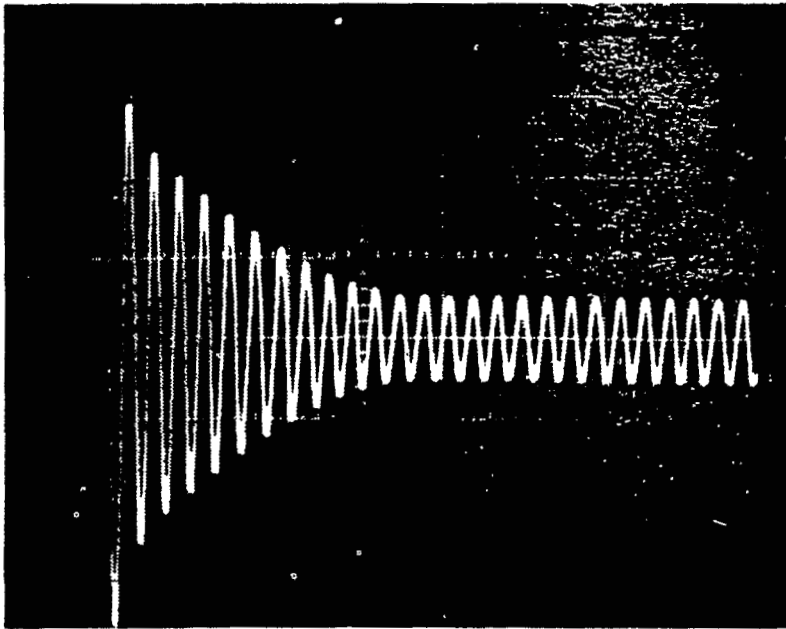
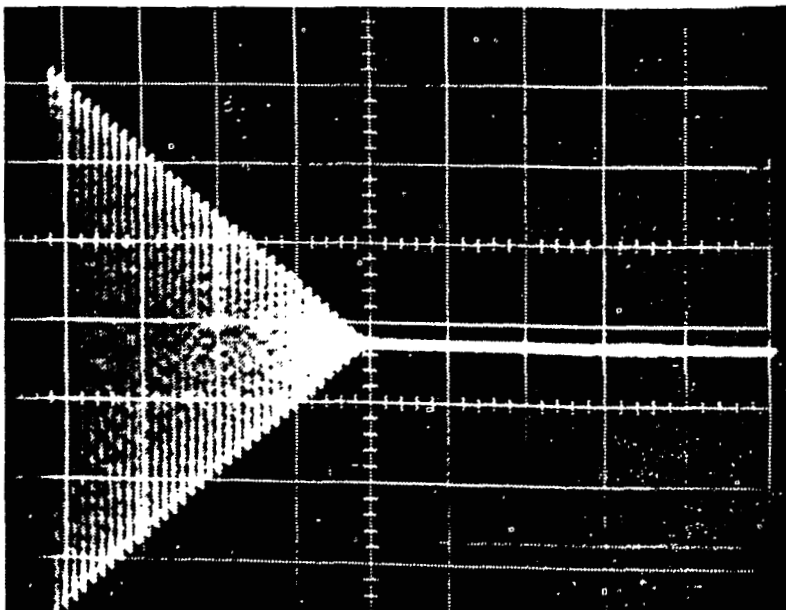


Fig. 10. Experimental method: calorimeter, using thermal conductivity of specimen (Ref. 5).



Two-component decay of voltage oscillations in superconducting L-C circuit. Time scale is 2 msec/div. Initial current was 2 mA.



Linear decay of voltage oscillations in superconducting L-C circuit. Time scale is 2 msec/div. Initial current was 100 μ A.

Fig. 11. Experimental method: decay of oscillations in superconductive L-C circuit (Ref. 84).

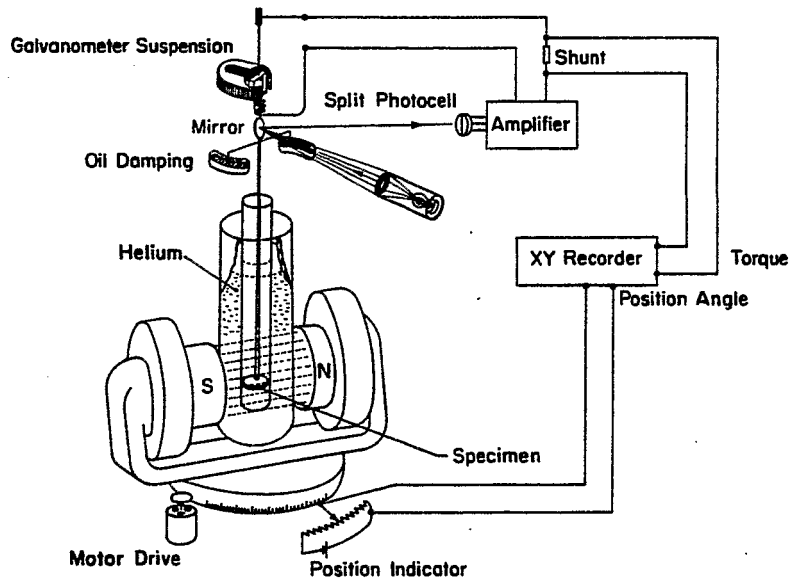


Fig. 12. Experimental method: flux pinning measured as torque which slowly rotating field exerts on specimen (Ref. 86).

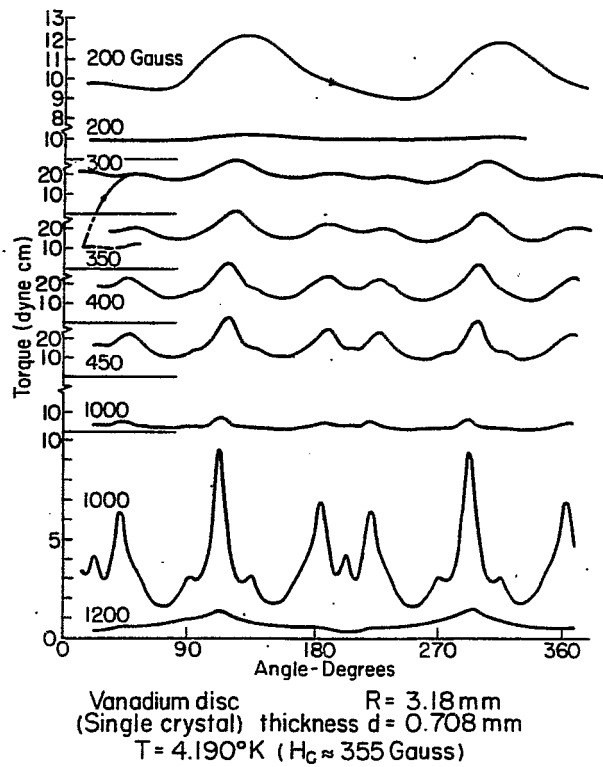


Fig. 13. Anisotropy of flux pinning in vanadium, measured with torque method (Ref. 86).

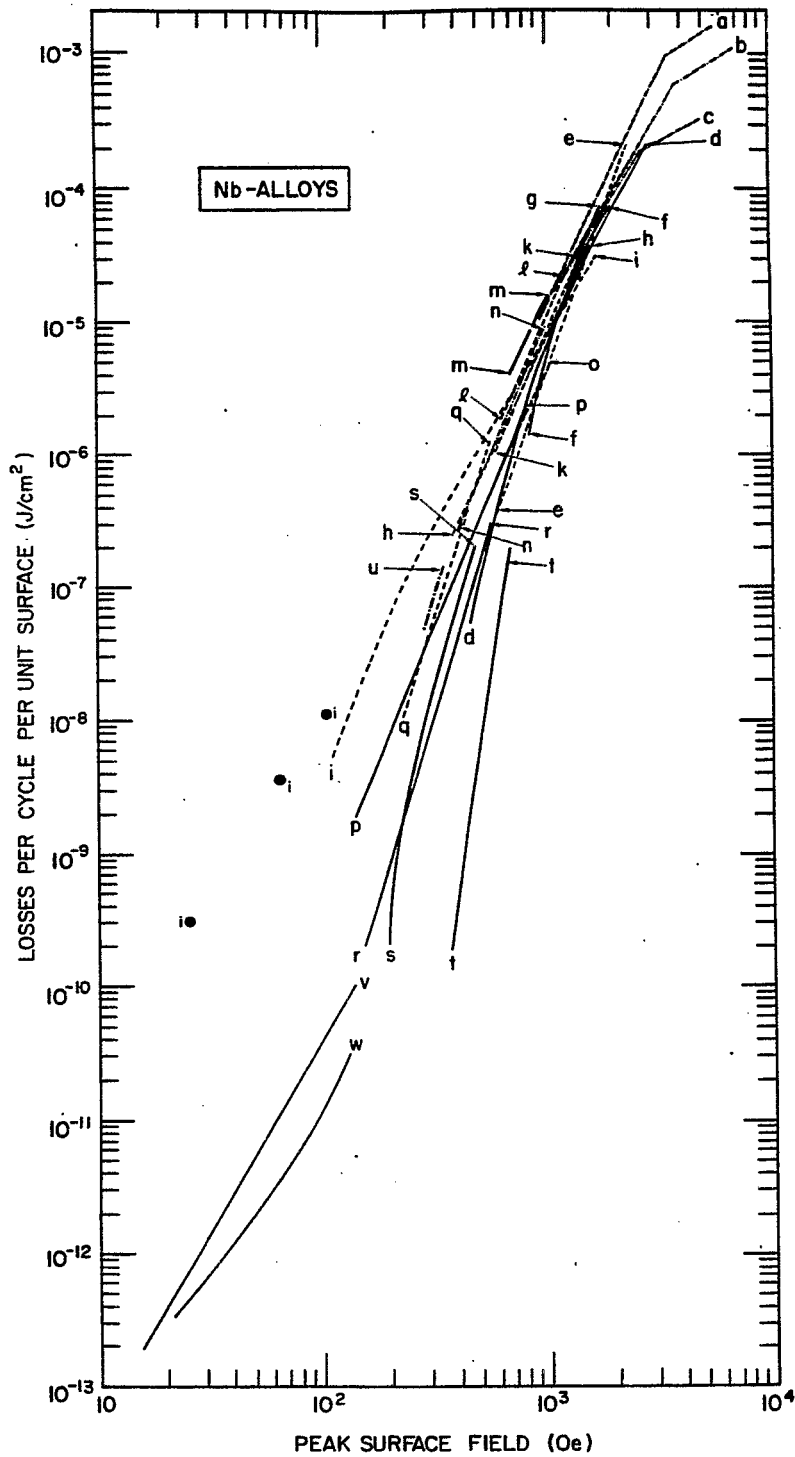
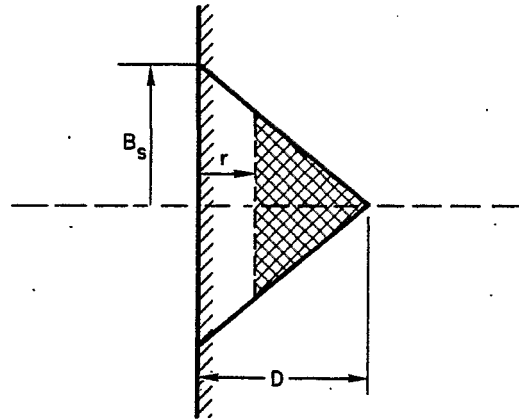


Fig. 14. Reported ac losses in NbZr and NbTi alloys (see Table IV).

Curves: ----- : bifilar coil (corrected for average field at the surface of the wire)
 ————— : single wire or widely spaced bifilar coil
 : other geometries (also corrected).

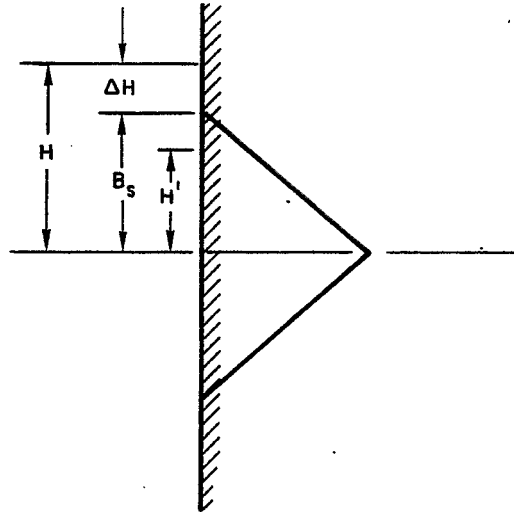
$$\iint \mathcal{E} j \, dt \, dv = \int_0^D \iint \frac{d\phi}{dt} j \, dt \, dr$$



$$2 \int_0^D B_s \left(1 - \frac{r}{D}\right) (D-r) j_c \, dr$$

$$= 2 j_c B_s \left(Dr - r^2 + \frac{r^3}{3D}\right) \Big|_0^D = \frac{B_s^3}{24 \pi^2 j_c}$$

Fig. 15. Loss per cycle by calculating the joule heating.



$$\text{LOSS PER CYCLE} = \frac{(H - \Delta H)^3}{24 \pi^2 j_c}$$

$$\text{FOR } j_c = 4 \times 10^5 \text{ A/cm}^2$$

$$\text{LOSS} = 1.05 \times 10^{-14} (H - \Delta H)^3 \text{ [JOULE/cm}^2\text{]}$$

H in Oe

Fig. 16. Modification of loss by the surface step ΔH .

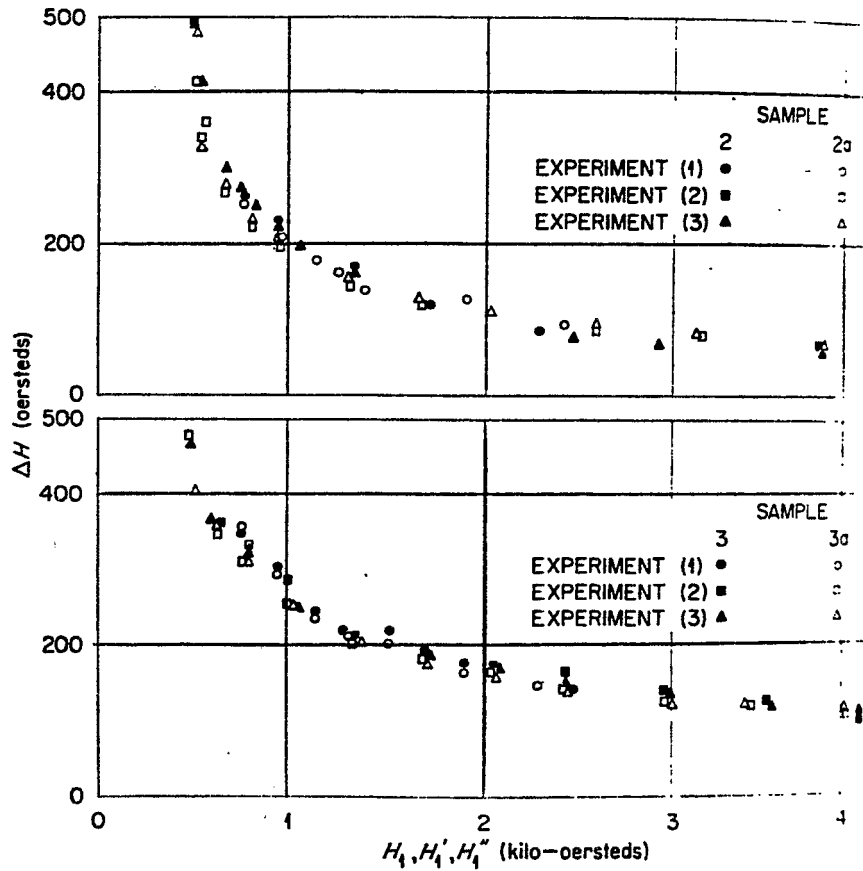


Fig. 17. Measurements of ΔH for Nb25%Zr (Ref. 79).
 Sample 2: diameter 0.68 cm; cold-worked, annealed and machined.
 Sample 3: diameter 0.63 cm; cold-worked, and mechanically polished.
 (The open symbols in both cases are for 30 μ silver-plated surfaces.)

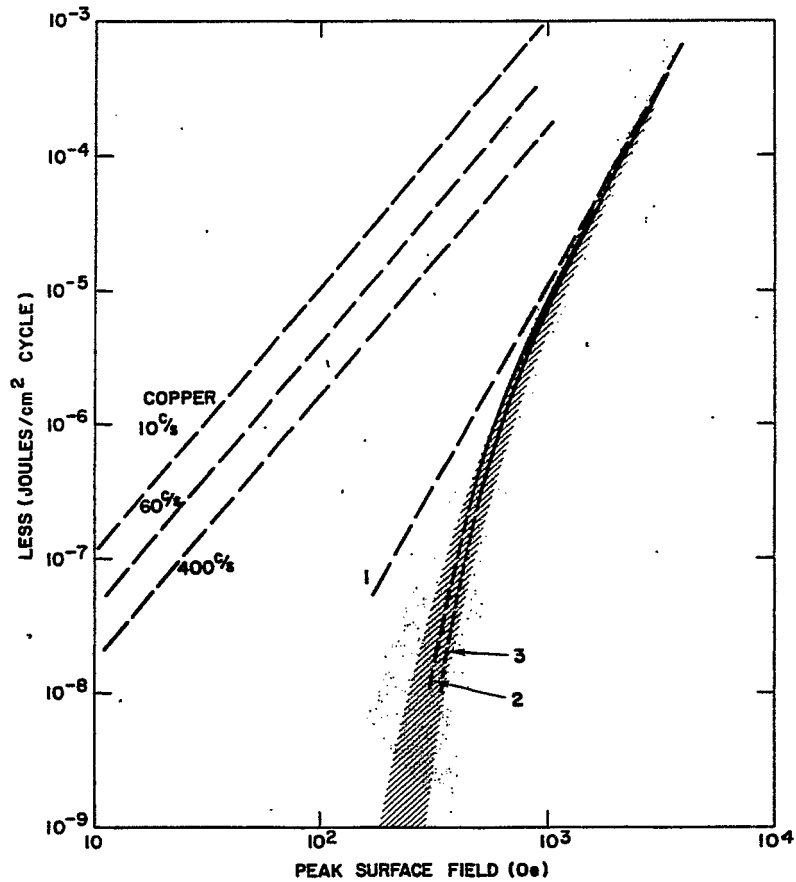


Fig. 18. Comparison of losses in Nb alloys with calculations.
 Curve 1: $\Delta H = 0$
 Curves 2 and 3: ΔH corresponding to sample 2 and 3 of Fig. 17.
 Shading indicates the portion of the curves in Fig. 14.
 Ac losses for copper ($10^{-8} \Omega \cdot \text{cm}$) are indicated for 10, 60 and 400 c/sec; the sample is assumed to be thicker than twice the penetration depth.

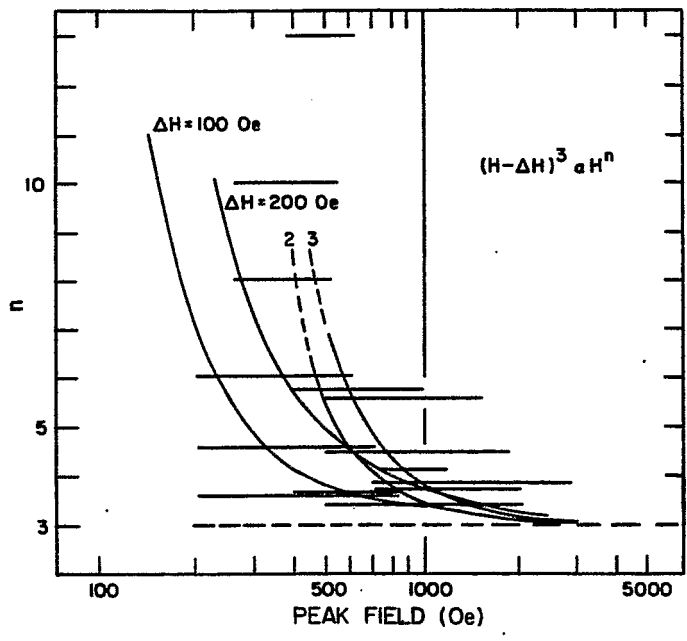


Fig. 19. Comparison between H^n and $(H - \Delta H)^3$. Horizontal bars indicate published values of n , relating to loss measurements over the indicated range of peak field.

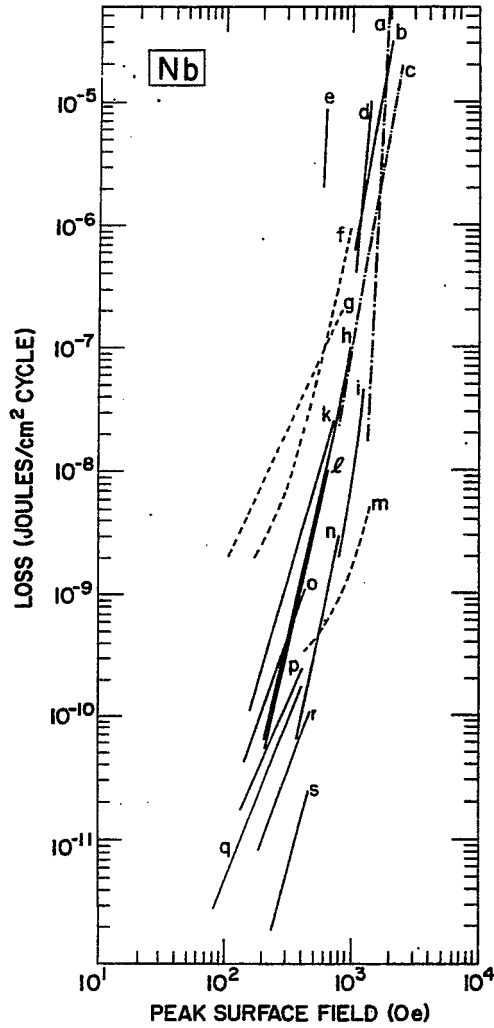


Fig. 20. Reported ac losses in pure Nb (see Table VI). Same curve symbols as Fig. 14.

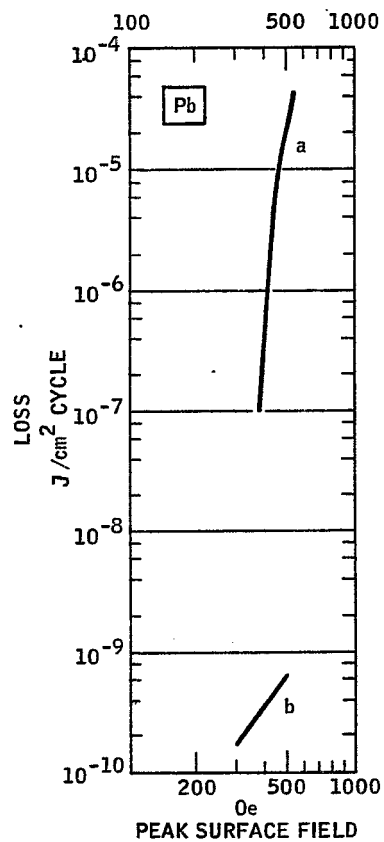


Fig. 21. Reported ac losses in pure Pb.
 Curve a: Ref. 8. Curve b: Ref. 2.

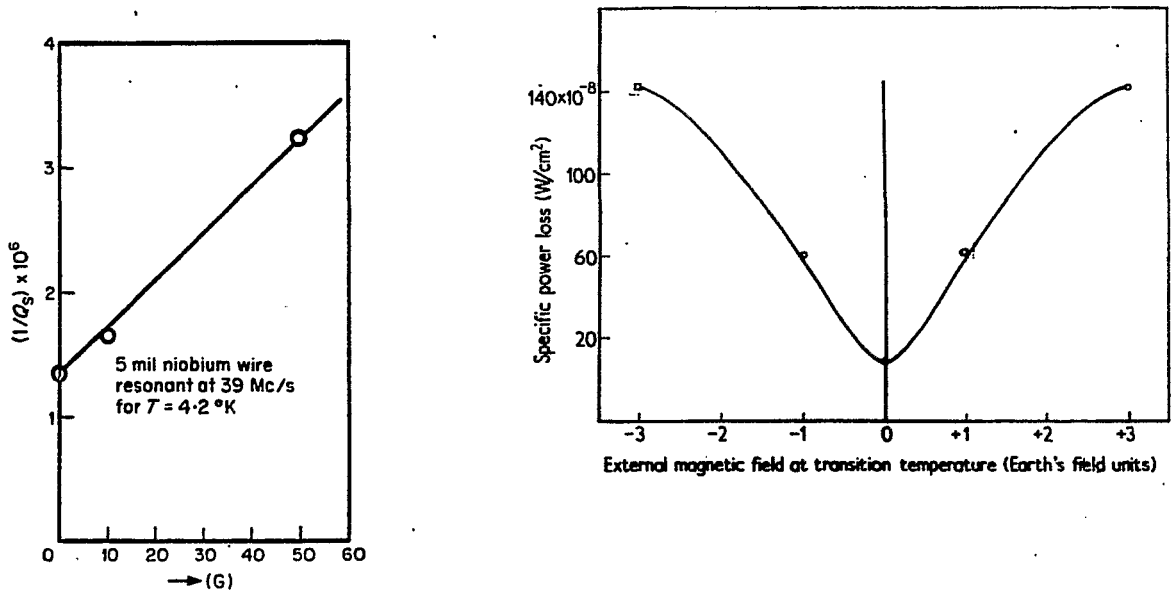


Fig. 22. Loss vs background field during cooldown for Nb (Ref. 71) and for Pb (Ref. 2).

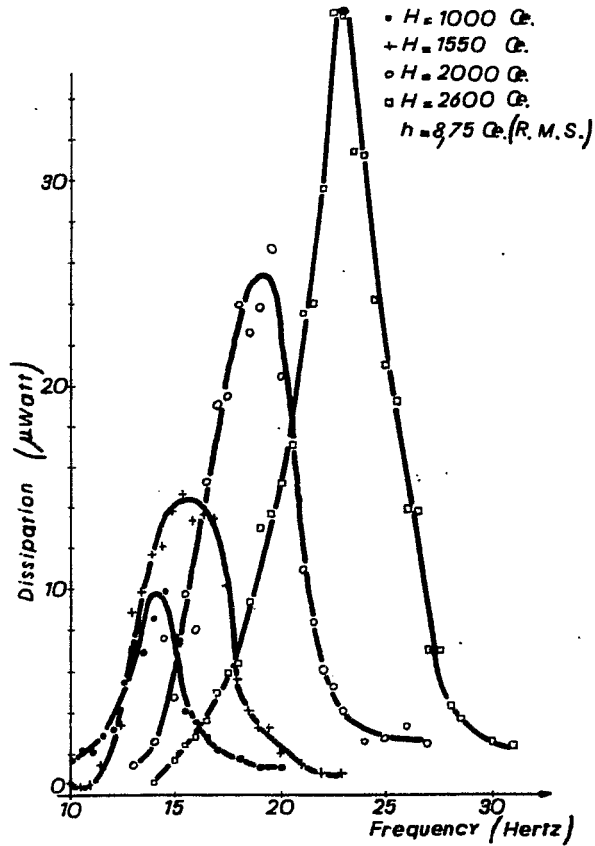


Fig. 23. Resonance of losses in pure Nb (weak pinning) (Ref. 80).

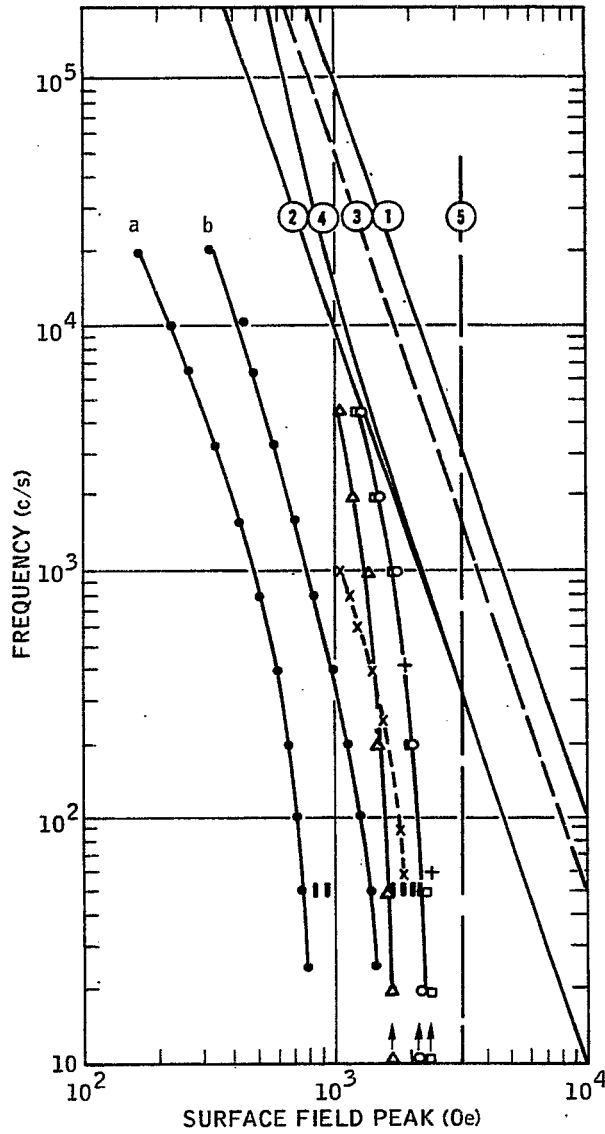


Fig. 24. Experimental ac critical currents plotted as frequency of the ac current vs the surface peak field created by the ac current. The points are referenced in Table VII. The curves numbered 1-5 are theoretical limits explained in the text.